Working Toward a Long-Term, Real-Time Measurement Network for Atmospheric Aerosol Sources

Olivia Hakan

A thesis

submitted in partial fulfillment of the requirements for the degree of

Master of Science in Applied Chemical Science and Technology

University of Washington

2023

Committee:

Joel Thornton

Robert Synovec

Program Authorized to Offer Degree: Chemistry

University of Washington

Abstract

Working Toward a Long-Term, Real-Time Measurement Network for Atmospheric Aerosol Sources

Olivia Hakan

Chair of the Supervisory Committee:

Joel Thornton

Atmospheric Science

Aerosols have a significant impact on both human health and the Earth's climate. Due to their complexity and variety, however, relatively little is known about them. ASCENT is a new aerosol measuring network that aims to fill these gaps in our knowledge. With 12 sites across the US, which each have an ACSM, Xact, SMPS, and Aethalometer, it is the most advanced large-scale, real-time network implemented in the field at this time. Though the project installation is still ongoing, UW's suite of instruments has already provided unique insight into rural pacific-northwest aerosol composition and sources. For example, both the ACSM and the Aethalometer were in use during a high mass-loading aerosol event seen in December 2022. By observing a high brown-to-black carbon ratio, the presence of the MS m/z 60 levoglucosan

tracer, and comparison with previous measurements, it was determined that the event was most likely a biomass-burning event. Non-negative matrix factorization (NNMF) was also proven to be a useful tool for analyzing large sets of data, which will be useful for instruments that collect such abundant data.

Table of Contents

1. Introduction

a. Background

The Earth's atmosphere is composed of a huge variety of chemical compounds that impact our everyday lives and our entire climate. Aerosols or particulate matter (PM) are one class of these species. Aerosols are small particles that are suspended in the atmosphere. They are highly variable in their size and composition and, therefore, their effects[33].

There are two main types of aerosols, primary and secondary. Primary aerosols are released directly into the atmosphere through biogenic or anthropogenic processes. Some examples would include desert mineral dust, volcanic ash, and black carbon from biomass-burning events. The different types of aerosols vary significantly in size, and because of these size differentials, their lifetime in the atmosphere also varies[2, 4].

Secondary aerosols are formed through gaseous reactions or condensation[14]. This process can occur through condensation onto existing particles or nucleation, which creates new particles. For example, isoprene, an abundant gas phase molecule in the atmosphere, reacting with OH can lead to particle phase products[20, 28]. Typically these aerosols are smaller in size than primary aerosols and therefore stay in the atmosphere for longer periods of time[33].

Once in the atmosphere, both types of aerosols impact our climate in a number of ways. Primarily, all aerosols scatter and reflect incoming solar radiation to some degree. This is responsible for some cooling of the atmosphere, as well as the presence of haze or decreased visibility. Some can also absorb solar radiation, most notably black carbon. This absorption results in the warming of the atmosphere. These are both considered direct effects of aerosols, and their net effect depends on composition, surface characteristics, and cloud cover[2, 4, 33].

Indirectly, aerosols can impact the climate by altering the size of cloud droplets and surface albedo and acting as sites for heterogeneous chemistry. Specific types of aerosols, such as sea spray and sulfates, can act as cloud condensation nuclei (CCN)[31]. In this process, aerosols help create a larger number of smaller cloud droplets which increases the cloud's albedo and results in a cooling effect. Contrastingly, though, if black carbon and/or other solar-radiation-absorbing aerosols are deposited on snow or ice, they can reduce the surface albedo, resulting in a warming effect[33].

The direct and indirect impact of aerosols on our climate can be caused by both biogenic and anthropogenic sources, but as we continue to alter our environment, understanding the ways in which we change these processes become even more complex and non-linear[25].

Additionally, it's not just our climate that is changed by aerosols; humans are also affected and, as a result, suffer from a variety of health ailments due to their impact. In general, smaller aerosols (PM<2.5 μm) pose the most risk to humans, as they have the ability to be inhaled deep into the lungs, and when deposited on the surface of the lung alveoli, they can be absorbed and potentially transported into the bloodstream. This exposure has been linked to heart attacks, asthma, respiratory irritation, decreased lung function, and death in vulnerable populations[43].

It is clear that aerosols have a large impact on our world. However, there is still a lack of information about aerosols compared to other atmospheric species and pollutants. In large-scale climate models, more than a handful of species are rarely considered, and the uncertainty in composition and source is still large[2, 33]. This is due to the large variety in aerosol composition as well as effect, in conjunction with relatively high complexity and low concentrations, particularly for SOA[8, 45]. In order to provide data for use in models, policies, and public

education, it is important that there are more studies specifically focused on aerosols, their compositions, and their effects.

b. Current Efforts

Within the field of atmospheric science and aerosol chemistry, there are a few main methods of measuring and analyzing aerosols which generally fall into two categories: instrument and satellite observations. Satellite data is usually collected using radiometers, which record aerosol optical depth (AOD) by measuring the amount of light that is scattered or absorbed. The higher the AOD, the more aerosols are present, and the hazier the sky will appear. This provides widespread data for use in analyses. However, these satellite-based observations tell us little about the composition of the aerosols they measure. Instrument-based observations, while time intensive and relatively stationary, can provide much more detailed information[2, 34].

At this point, most instrument-based aerosol measurements are acquired through short-term field campaigns. In these campaigns, instruments are brought to a field site or fitted into airplanes and measure for only the duration of the campaign, which may last anywhere from days to months. These programs certainly have been crucial in much of our understanding of aerosol chemistry, but they still only collect data from one location for a short period of time and can, therefore, only represent the aerosol concentrations and conditions for that specific project. This presents the problem of a lack of long-term data collection that would allow access to information far beyond the scope of these limited field campaigns[34].

In the US, three major networks have been implemented to try and solve this issue. The Interagency Monitoring of Protected Visual Environments (IMPROVE) network was developed in 1985 as a set of 30 stations, mostly based in national parks, to monitor the visibility issues caused by anthropogenic pollution. In 1999 another 110 sites were added to collect data on

regional areas. Each of these sites collects 24hr averaged samples every three days, which include measurements of PM2.5, PM10, sulfate, nitrate, chloride, and elemental carbon concentrations[22].

The Chemical Speciation Network (CSN) was developed in 1997 to establish a PM2.5 network across the USA. There are 50 full sites and another 110 supplemental sites currently, and each collects PM samples on three different filters. They collect and analyze Teflon filters for 33 different element concentrations, nylon for ion concentration and quartz for carbon concentration. The full sites measure one in every three days, and the supplemental measure one in every six, with all of the sites collecting 24hr averages[44].

The National Core multipollutant monitoring program (NCore) began operating in 2011 as a way to advance pollutant measurement and consists of eighty sites across the US. Each site records PM2.5 speciation and concentration, and PM2.5-10, ozone (O3), carbon monoxide (CO), sulfur dioxide (SO2), nitrogen oxide (NO), and total reactive nitrogen (NOx) concentrations, as well as wind speed, temperature, and relative humidity (RH)[35].

These networks, while extensive in their locations and major advancements in the field, still only record a small number of species, none of which include organic aerosols, and are largely filter based. While filter-based instruments do produce reliable and accurate results, they are laborious, requiring staff to collect the samples, and must be analyzed off-site. This results in delays in data acquisition, on top of the 24-hour averages already performed by the instruments. For example, IMPROVE data can take six months to an entire year to be added to their online database, and in the averaging process, aerosol events can be missed. Additionally, the data is unable to differentiate between organic species, which make up a significant portion of particulate matter, and therefore lack information on source apportionment[9, 17].

Since the deployment of these networks 10-20 years ago, the technology we use to measure aerosols has improved drastically. This removes the need for filter-based technology and allows for near-real-time online data access.

At this point, the only major real-time, continuous aerosol networks are not in the US. Two examples are The Aerosol Clouds and Trace gases Research InfraStructure network (ACTRIS) and The National Aerosol chemical Composition MOnitoring Network (NACMON). ACTRIS, also established in 2011, is a European aerosol network with 110 sites across Europe that measure the hourly aerosol composition and trace gases[7]. While NACMON has sites in 31 Chinese cities and acquires hourly measurements of water-soluble ions, organic carbon, and elemental carbon[12]. In seven of these cities, they also measure trace metals, size distribution, and mixing states. Both of these networks have proven the utility of long-term, real-time measurements revealing specific diurnal profiles at different sites, as well as different compositions in high and low PM loading events.

The Atmospheric Science and Chemistry mEasurement NeTwork (ASCENT) has been developed as the US's counterpart to these networks to expand the conditions we collect data from and advance the field overall.

c. ASCENT

ASCENT is a network of twelve advanced aerosol measuring field sites located across the United States (*Figure 1*). These sites encompass a large variety of geographical elements, ranging from inside large cities to the deep south to rural Alaska, ensuring there will be variation in conditions and aerosol sources. Each site will be equipped with an Aerosol Chemical Speciation Monitor (ACSM), a Xact multi-metals monitor, an Aethalometer, and a Scanning

Mobility Particle Sizer (SMPS). This project is funded by the NSF and is currently in its first year of installation/operation.

From these four instruments, researchers will be able to access knowledge about long-term aerosol trends, variability in composition, and short-term aerosol events. The network's goals are to establish a long-term, real-time, high-resolution aerosol measuring network to advance atmospheric science, impact policy change, and more fully utilize upcoming satellite-based observations. To develop frameworks for aerosol measuring protocols and databases, improve training for students and professionals, and support national and worldwide atmospheric observation research[1].

This network will all allow for the differentiation between organics, source apportionment of aerosol species, and analysis of diurnal and spatial profiles between sites leading to the improvement of data inventories and models, more accurate development of air quality regulations, and a better understanding of human and environmental health impacts.

2. Instrument & Installation

a. Cheeka Peak Field Site

The University of Washington's ASCENT site is colocated at a current IMPROVE/NCore site at Cheeka Peak Observatory (CPO) on Makah Tribe land (*figure 2*). Cheeka Peak is on Washington's Olympic Peninsula, near Cape Flattery. Its closest significant city is Port Angeles, 75 miles east, making it very rural. The network has designated the site as a clean marine background, and we expect to see very low aerosol concentrations for the majority of the sampling period. However, there are still plenty of opportunities for aerosol events to occur. Being only 5 miles from the Pacific Ocean and the Strait of Juan de Fuca, there is the possibility of observing ship traffic emissions as well as long-range transport of mineral dust, pollution, and biomass burning from Asia and Siberia[6, 21]. Additionally, as it is in the pacific northwest, there will certainly be smoke from the summer fires in Washington, Oregon, and British Columbia that makes its way to the site[15, 18].

The preexisting setup of the site includes three trailers containing the equipment used for the IMPROVE and NCore networks. The ASCENT instruments were installed in the NCore trailer (*figure 4*).

CPO was also historically used as a field site for Daniel Jaffe's group at the University of Washington to study air pollution and long-range transport of aerosols[21].

b. ACSM

The Aerosol Chemical Speciation Monitor (ACSM), manufactured by Aerodyne, analyzes aerosols using time-of-flight mass spectrometry (ToF-MS). The instrument operates in

two modes, filter mode, and sample mode. A three-way valve controls the mode to enable sample air to reach the instrument (when in sample mode) or to send the air through a filter and have particle-free air enter the instrument (when in filter mode.) This is done to measure background signal levels[37].

In sample mode, after aerosols enter through the ACSM inlet, they are focused into a beam using a 75-650nm aerodynamic lens fitted with a critical orifice of 100 μm. This beam is then transmitted through a vacuum chamber where gas is separated from the particles using differential pumping via turbomolecular and diaphragm pumps. The particles are then flash vaporized by a heated tungsten surface and ionized using 70ev electron impact ionization so all particles have the same charge[13, 37].

These ions are injected into the time-of-flight (ToF) mass spectrometer, where they are accelerated through the flight chamber using an electric field. The ions are separated in this process based on their mass-to-charge ratio, meaning the smaller the ion, the more quickly they fly through the tube and impact the detector. This flight time is transformed into a spectrum of m/z and related back to the different aerosol species using fragmentation patterns. This signal is also converted to mass loading to provide overall concentrations for each category of aerosols, organic, sulfate, nitrate, ammonia, and chloride[13, 37].

There are a number of calibrations needed for the ACSM to produce accurate and analyzable data. Primarily, ammonium nitrate is used to calibrate the instrument signal since it vaporizes with complete efficiency. In order to perform the calibration, an atomizer is needed to generate ammonium nitrate particles, which are then size selected with a particle counter. The mass of these particles is calculated, and the response factor (RF) of NH4/NO3 is used as the relative ion efficiency (RIE)[37].

The reason the ASCENT network chose the ACSM as one of its four instruments is primarily due to its near-real-time continuous monitoring capabilities. The instrument switches between sampling 40s and filtering 20s, giving almost minute data on aerosol composition. It can measure aerosols from 0.04-3.5 μm and has detection limits of 0.03-0.06 $\mu m/m^3$, depending on the species measured. Though it only has a 2000 m/dm mass-to-charge resolution, its speed and the wealth of information provided compared to filter-based instruments more than make up for the lower resolution considering the goals of ASCENT[13, 37].

The ACSM was installed at the University of Washington's field site, CPO, to the ASCENT specifications displayed in *Figure 3*. This installation included drilling an inlet in the trailer roof to pass the ⅝" tubing through. A PM2.5 cyclone was installed at the end of the inlet, and a Nafion dryer is located upstream of the instruments to ensure the sample air is dried uniformly. This inlet is used for both the ACSM and the SMPS, with a ¼" Y-splitter downstream of the Nafion dryer, diverting the air between the two. This setup allows for the calibration of the ACSM to be done using the SMPS without having to modify the inlet. All tubing is McMaster Carr stainless steel (SS 316), and all tubing connectors are Swagelok stainless steel (SS). The inlet extends 2m above any obstructions, and bends in the inlet were minimized to prevent particle loss. The instrument was run as described in Ng. et al., and the 1-minute data points were averaged every 10 min[37].

c. Scanning Mobility Particle Sizer

The Scanning Mobility Particle Sizer Spectrometer (SMPS) (model 3938), manufactured by TSI, measures the total concentration of aerosols in a sample as well as their size distribution. This instrument is composed of two different units: an electrostatic classifier (EC) (model 3082) and a condensation-based particle counter (CPC) (model 3789)[24].

When the sample air enters the instrument, it first encounters an impactor, which removes large particles by drawing the sample through a series of jets with decreasing diameters. This polydisperse aerosol sample then travels to the electrostatic classifier, where a krypton-85 neutralizer brings the sample to thermal charge equilibrium. A differential mobility analyzer (DMA) is then used to produce an electric field that allows only particles of a certain mobility to exit with a monodisperse charge and flow into the CPC[25].

The CPC uses supersaturated water vapor that condenses onto the aerosol to grow the sample to optically detectable droplets. These droplets then flow into an optical laser diode detector, where they scatter light that can be detected by the diode. This is then converted into electrical pulses and counted to give the particle concentration. The SMPS is formed by connecting the DMA monodisperse aerosol outflow to the CPC sample inlet[25].

Calibration of the SMPS is done by looking at the flow rate with a flowmeter, verifying the voltage with a high-voltage probe, and checking the particle sizing using 150nm latex standard-size particles. To maintain the instrument's function, cleaning the impactor nozzle and changing the water reservoirs are also required periodically[25].

The SMPS was chosen for the network as it allows for more detailed information on the size distribution of the aerosol sample (2.2-1000 nm) and, since it is measuring all species, provides the total concentration of all <PM2.5 aerosols between 1 and 10^7 particles/cm^3. This is a good comparison for the values recorded by the other instruments, and with the size distribution over time, it is also possible to see new particle formation occur, particularly in clean background areas[40].

The Installation process for the SMPS at CPO was identical to the ACSM since their flows are split. This was shown in *Figure 3*. The instrument was run at 6 L/min flow and -0.6V for the DMA voltage.

d. Xact Multi-Metal Monitoring System

The Xact Multi-Metal Monitoring System 625i, manufactured by Cooper Environmental, measures the concentrations of 46 different metals simultaneously. When sample air is drawn into the instrument, it is exposed to a filter tape. The inlet tube is heated, causing particles to collect on this filter. The tape is advanced toward the X-ray tube, and the sample is irradiated using X-ray Fluorescence for analysis. When the particles are irradiated, they lose an electron, and a vacant orbital is left. A higher energy electron will drop down to fill this vacancy, and fluorescence emission will occur as a result of the transition. This energy is characteristic of each element and acts as a fingerprint. The observed fluorescence is recorded and counted by the detector so they can be sorted by energy level, producing a spectrum of metal concentrations[46].

There are a variety of calibrations and maintenance tasks also needed for the Xact to perform. Primarily, the filter tape needs to be changed roughly every 30-60 days, and a tube seasoning must be performed after the instrument has been off for more than 24hrs to ensure the X-ray tube remains functioning properly. Additionally, after transport, or quarterly, the instrument needs an Xrf check; this involves using five standards to make sure the calibrations remain accurate, as well as flow and leak checks to ensure the flow from the pump remains at the correct values. Once a year, it is also necessary to replace the X-ray tube. After each replacement, all 44 standards need to be run to calibrate the new tube initially[46].

Due to a tube that failed early, all of these calibrations were performed on the UW Xact before transport to the site.

Unlike the other three instruments, the Xact measures only metal concentrations. This is a fairly unique measurement in the field and provides an entirely new category of data for most of the ASCENT sites. Though it is filter based, the instrument measures all 46 metals simultaneously and uses an auto-advance system every hour. So, unlike the NCore and IMPROVE filter-based instruments, the concentrations are hourly rather than daily, and the only time the filters need to be changed is on a monthly/bimonthly schedule when the tape runs out. Additionally, the detection limits range from low pg/m^3 to low $\mu g/m^3$ depending on the metal, which allows for the detection of even low-concentration metals[46].

The Xact was installed at CPO to the specifications indicated in *Figure 4*. This setup was fairly simple and required only drilling an inlet hole in the trailer roof and securing the metal tubing, as well as installing the PM2.5 size selector at the end of the manufacturer-included 1.5in tubing and adding insulation around the tube just above the instrument. Similar to the previous inlets, the tubing ended 2m above any obstructions. The instrument was run with the 16.7 L/min flow.

e. Aethalometer

The Aethalometer, model AE33-7(AE33), manufactured by Magee Scientific, provides real time concentrations of light-absorbing aerosols, most notably black and brown carbon. When sample air flows into the instrument, particles are trapped using a filter. A beam of light is transmitted through the filter, and radiation-absorbing aerosols attenuate the light projection. The sample light transmission is compared to that of a clean reference filter for seven different wavelengths. This absorption is proportional to aerosol concentration, so with the additional knowledge of flow rate, the concentration of optically absorbing particles is calculated and reported[19].

In order to keep the aethalometer running effectively, the optical chamber should be cleaned twice a year with ethanol, and when the filter tape runs out (the time depends on black carbon concentrations at various field sites), it must be changed. Flow calibrations can also be performed as needed using a flow meter[19].

Though fairly simple compared to the other three instruments, the aethalometer provides unique insight into the concentrations of optically absorbing aerosols in near-real-time measurements of seven wavelengths between 370 and 950 nm. This includes black and brown carbon, related to wavelengths 370 and 880, respectively, and has implications for biomass burning. The limit of detection is under 0.005 $\mu g/m^3$, and due to its simplicity, it makes for a great instrument to be used in remote sites or where local operators will have to be checking on the instruments rather than technicians or other scientists[19].

The AE33 installation diagram is shown in *Figure 5*. A Nafion dryer was installed similarly to the ACSM/SMPS inlet to ensure the sample air is uniformly dried between instruments and sites, and a PM2.5 cyclone was installed at the end of the tubing, 2m above obstructions. The tubing was McMaster Carr stainless steel (SS 316), and the connectors were Swagelok stainless steel (SS). The instrument was run at 5.0 L/min.

3. Data & Analysis

a. Aethalometer

UW's aethalometer sampled from September 2022-October 2022 in the Thornton lab on campus and from December 2022 onward at the CPO field site. This time series is shown in *Figure 6*, where the gap in data occurred during the installation period. The values between the Seattle-based data and the field site data are clearly very different, with the average values in Seattle falling around 4 $\mu g/m^3$ and 0.1 $\mu g/m^3$ at the CPO site. Fall of 2022, Seattle had the worst air quality of any major city in the world due to smoke transported from wildfires, which is reflected in the extremely high black and brown carbon values of 2-15 ug/m^3 [39]. The method used to calculate the brown carbon value is described in Olson et al.[38]. In contrast, when the instrument was transported out to the field site, the values drop down significantly for the majority of the data collection period.

Figures 7, 8, and *9* plot the diurnal cycles of black carbon at UW and CPO. Once again, a clear daytime elevation can be seen at the UW site (*figure 7*), indicating that there is an additional increase in black carbon due to fossil fuel combustion as well as smoke transport. There was no clear daily pattern in the wintertime at CPO (*figure 8*), which could have been impacted by the relatively large spikes of PM during December. In the spring (*figure 9*), however, the diurnal profile is almost an inversion of what was seen in Seattle. The relatively higher black carbon levels during the nighttime at CPO could be indicative of heating sources in the Neah Bay area [32].

b. Xact

Due to shipping delays and instrument errors, the Xact has only sampled air from inside the Thornton lab in Seattle. Even so, the data is promising. *Figure 10* shows a brief concentration time series of three metals commonly found in urban environments over the course of January 2023. There are a few obvious spikes and patterns that could indicate a correlation with traffic, human presence in the lab, and/or weather. In particular, the diurnal cycle of Copper in January (*Figure 11*), which is known to be found in urban dust as well as soil, shows elevation during the daytime hours when people are most likely to be present in lab [3]. Once the Xact data from the CPO field site is acquired, ship traffic emissions are expected, which are often characterized by vanadium and nickel [10, 49]. Dust transport from Asia, which often contain elevated levels of copper. lead and zinc, among other heavy metals, is also expected [29]. Additionally, since the metals measured in Seattle are so low already, a higher averaging time period will be tested at the field site to obtain more reliable values.

c. SMPS

Similarly to the Xact, due to shipping delays, only a few days of CPO data was collected from the SMPS. However, even with the limited data, there is still great potential for analysis from the information provided. *Figure 12* (top) shows a plot of particle concentration (in dN/dlogDp) vs. diameter. This allows for the observation of particle sizes and frequencies. The bottom displays the total concentration (in particles/cm^3) over the same time. Correlating these two together shows us that there was an increase in small particles sometime during the evening of 3/28/2023. In the future, new particle formation events that happen at the CPO site are expected. If the data is plotted in the same way, this would look like a large streak of high-concentration small particles changing to large particles over time[41]. These events are

important as they are a source of new aerosols and multi-phase chemistry and have been observed in a variety of locations, including coastal areas, forests, polluted cities, high altitudes, and polar environments[26].

d. ACSM

The ACSM was installed at the CPO field site in November 2022 and sampled from November 17-December 26, as well as from March 22, 2023, onward. A typical organic aerosol time series and diurnal cycle of organic aerosols for the area can be seen in *Figure 13*, where data from the first week in April 2023 is plotted. During the November installation, however, three wildfires broke out around Neah Bay[23]. The location of these fires is shown in *Figure 14*, and they were started by uncontrolled slash-and-burn piles that spread due to high winds (*figure 15*). The fires were put out by helicopters the next day. The organic aerosol time series of this event can be seen in *Figure 16*. These fire signals were clearly detected during the night of November 16th and the morning of November 17th, with high organic mass loadings.

In December 2022, there was another aerosol event that caused high levels of organic mass loading. The full December time series of all particulate matter compared with the aethalometer values is displayed in *Figure 17*, where the two spikes in concentration match almost perfectly. Unlike the November aerosol event, there was no news coverage or documented uncontrolled burns. However, it is still very likely that the event was caused by some sort of nearby biomass burning. Evidence that suggests this source is displayed in *figures 18-22* and expanded upon below.

Similarly to the November fire, the wind carrying most particulate matter came primarily off of the coast (*figure 18*) in December, and there was moderate wind speed and no precipitation recorded in the area during the event, meaning if there were burn piles from logging, smoke

could have been carried to the site rather than being put out by rain. Additionally, *figure 19* shows the aethalometer time series of the same dates, where it is clear that there is a high ratio of brown to black carbon. This is a primary indication that the event was also due to biomass burning[48]. From there, the mass spectrum (MS) of each event was compared with each other as well as with a clean background spectrum.

In previous studies, fossil fuel combustion-related, hydrocarbon-like organic aerosol (HOA) has been linked to MS fragments m/z 55 and 57 dominating the spectrum. Oxidized or aged OA (OOA) corresponds to high levels of m/z 44, while fresh primary OA (POA) is indicated by low levels of m/z 44. And biomass burning OA (BBOA) is characterized by the presence of m/z 60, as well as m/z 29 and 73 to a lesser extent. However, m/z 29 (and 27) are also seen at high levels in secondary OA (SOA)[11, 27, 36].

In the mass spectrum comparison, *Figure 20,* an enhancement of m/z 60 is observed in the December aerosol event as compared to the background December data. A comparison between the two events (*figure 21*) shows that while they have different overall concentrations, their signals and defining traits are remarkably similar as well.

M/z 60 is used as a BBOA tracer since it is a major fragment of the molecule levoglucosan, which is emitted from wood and biomass burning[5, 16, 30]. Each of these tracer fragments was plotted in a time series in *Figure 22.* In this figure, it is clear that while the event caused all particulate matter to increase dramatically, BBOA is only detectable during the event, while other categories of OA also appear at other times. For example, there are distinct spikes in the HOA concentration on and around December 22 and in the OOA between the 18th and 19th. Between BBOA tracers being only observed during the aerosol event in high concentrations and enhanced levoglucosan tracers, a nearly-identical MS to the previous fire, and the high

brown-to-black carbon ratio, it is likely that the December event was a fire similar to the slash-and-burn piles incited in November.

To analyze the time series further, non-negative matrix factorization (NNMF) was performed on the December 2022 time series in Matlab. Though it is clear that the large OA peak was caused by biomass burning, the ACSM produces an abundance of data, and such a lengthy analysis will not be possible for the full time series when it is continuously monitoring. NNMF is a technique often used to apportion distinct sources to a large data set[47]. In this method, an *n x m* matrix is introduced where *n* is the number of data points, and *m* is the number of chemical species. For the ACSM data, 35 different significant organic species were chosen as analytes. An optimal factorization rank, *k,* is also chosen by the user. After running several different ranks, an optimal rank of 4 was decided for this data set. NNMF extracts basis components (G matrix) and mixture coefficients (F matrix) for each factor, where GF would approximate the original data set X. This allows a complex set of data to be explained by a basic set of factors[42].

Two different NNMF schemes were run for the ACSM data in Matlab, one where the December event was selectively analyzed and one where the event was completely masked. The G matrix was plotted as a time series, and the composition of each of these factors (F) is shown for the two sets of data as a pie chart of the weight of each fragment in *Figure 23*.

In part *a* of *Figure 23*, factor 1 (F1) is clearly located in the later half of the fire peak, and in part a.1, we can see that F1 is mainly composed of HOA (purple) and OOA (blue), with a small amount of "other" (yellow), which is an uncategorized conglomeration of both low and high m/z that frequently occur in OA samples. This indicates that the aerosol is aged, which aligns well with the time series. F2, however, is almost entirely composed of BBOA. Looking at the G matrix time series, F2 occurs in the first half of the signal, and if we compare this to the

BBOA time series in *Figure 22,* it corresponds nicely with the m/z 60 and m/z 73 BBOA tracers. F3 and F4 are quite similar to each other, which could mean that a factor rank of 3 would have been able to describe the data set adequately. Both are composed of a mixture of HOA, Other, and BBOA and appear at background levels in the time series.

In part *b* of *Figure 23*, the background spectrum for December was analyzed, with the fire peak masked. F1, which is primarily clustered around the masked dates, is also significantly made up of BBOA. F2 is mainly uncategorized, similar to F4, and both seem to exist at relatively low background levels for much of the spectra. F3, in contrast, is made up of mostly HOA. If we refer back to *Figure 22,* HOA has discernable periodic spikes that are distinct from the other categories. In *Figure 24*, the diurnal cycles of each category are plotted, and the HOA trend has a slight increase in the daytime hours. This could indicate transport from local sources or vehicle visits to the surrounding areas and/or site.

Conclusion

Although the ASCENT project is still underway and not fully developed, initial results already provide unique insight into aerosol sources and composition. Once installed and continuously acquiring data, the SMPS and Xact have the potential to collect information on new particle formation events and ship traffic or transported pollution, respectively. The Aethalometer has already proven to give a clear comparison of urban vs. rural light-absorbing aerosol trends as well as giving insight into organic aerosol sources. The ACSM can provide a wealth of knowledge in even a few days of data, and with the proper analysis, can be used to not only record aerosol species but also allow researchers to distinguish aerosol sources and events with much more detail and accuracy than the existing framework for long-term measuring sites.

Figures

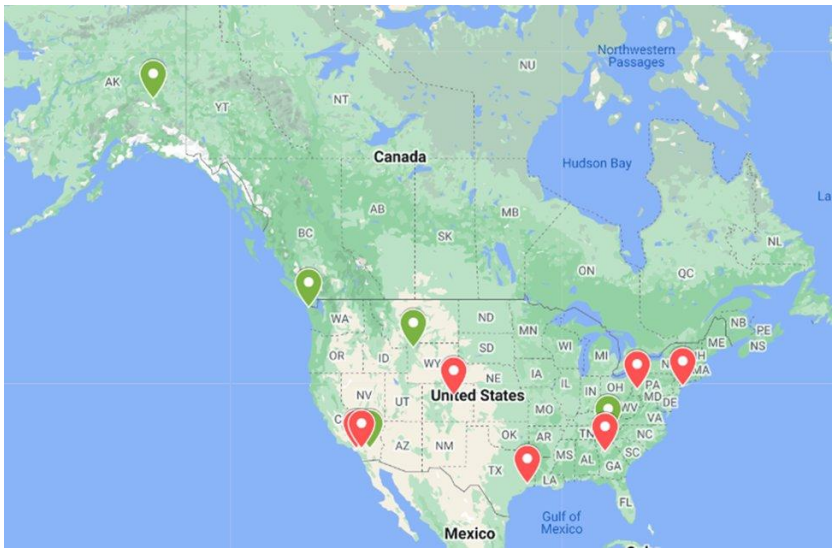

Figure 1: The twelve locations of the ASCENT sites. Red indicates an urban site, while green indicates a rural or background site.

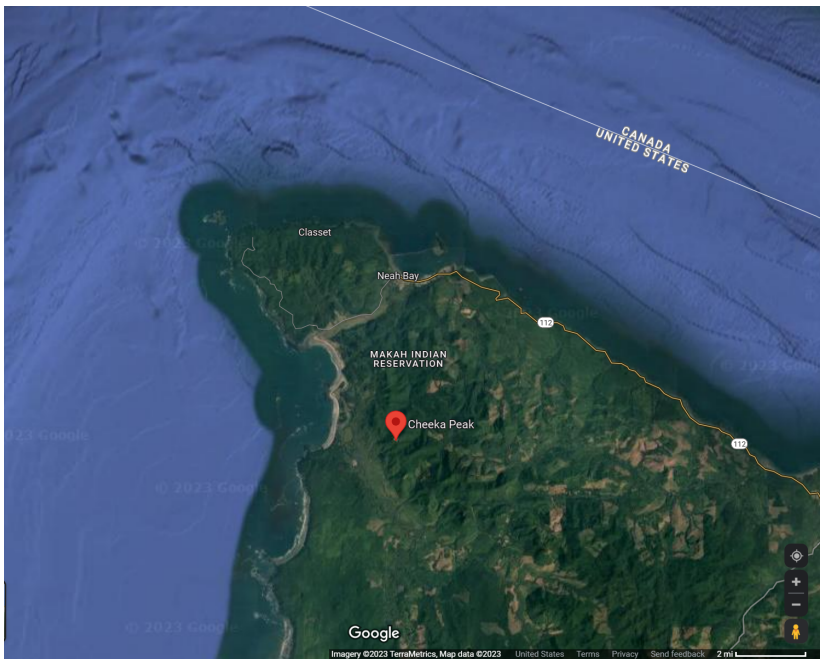

Figure 2: The Cheeka Peak field site is indicated by the red pin. The map is focused on Washington's Olympic peninsula.

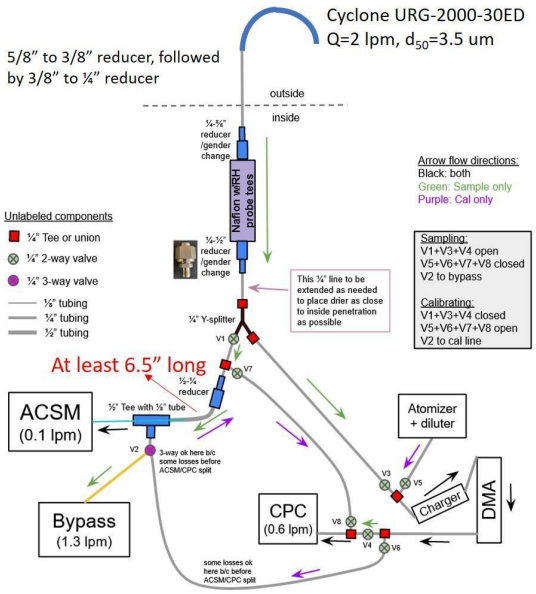

Figure 3: ACSM installation setup. A Nafion dryer was installed upstream of both instruments, and a PM2.5 cyclone was installed at the end of the inlet to filter out larger particles. The flow was diverted between the ACSM and SMPS using a Y-splitter as well as an optional bypass in order to use the SMPS to calibrate the ACSM when needed.

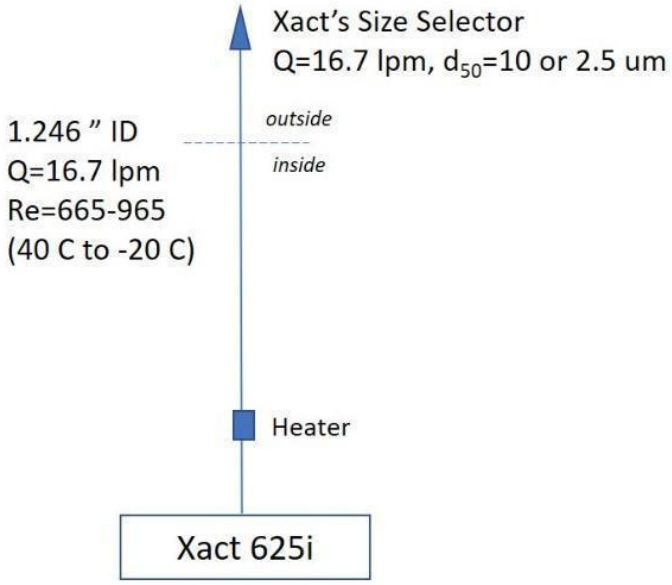

Figure 4: Xact installation setup. A heater was installed just above the instrument, and a PM2.5 cyclone was installed at the end of the inlet.

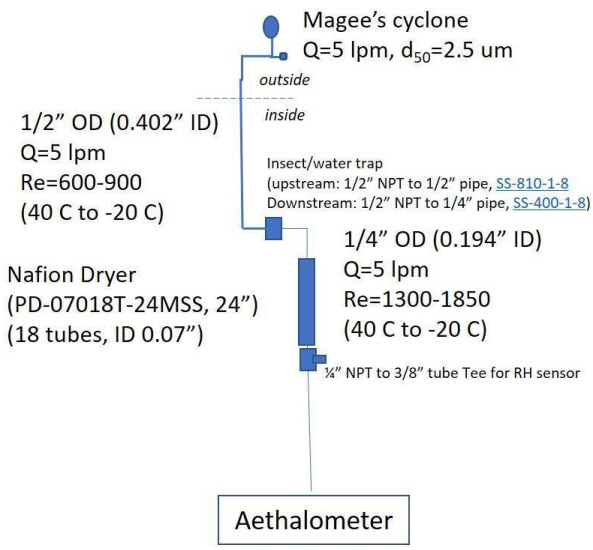

Figure 5: Aethalometer installation setup. A Nafion dryer was installed upstream of the instrument as well as a pump to run the dryer's purge flow, and an insect/water trap was installed upstream of the dryer.

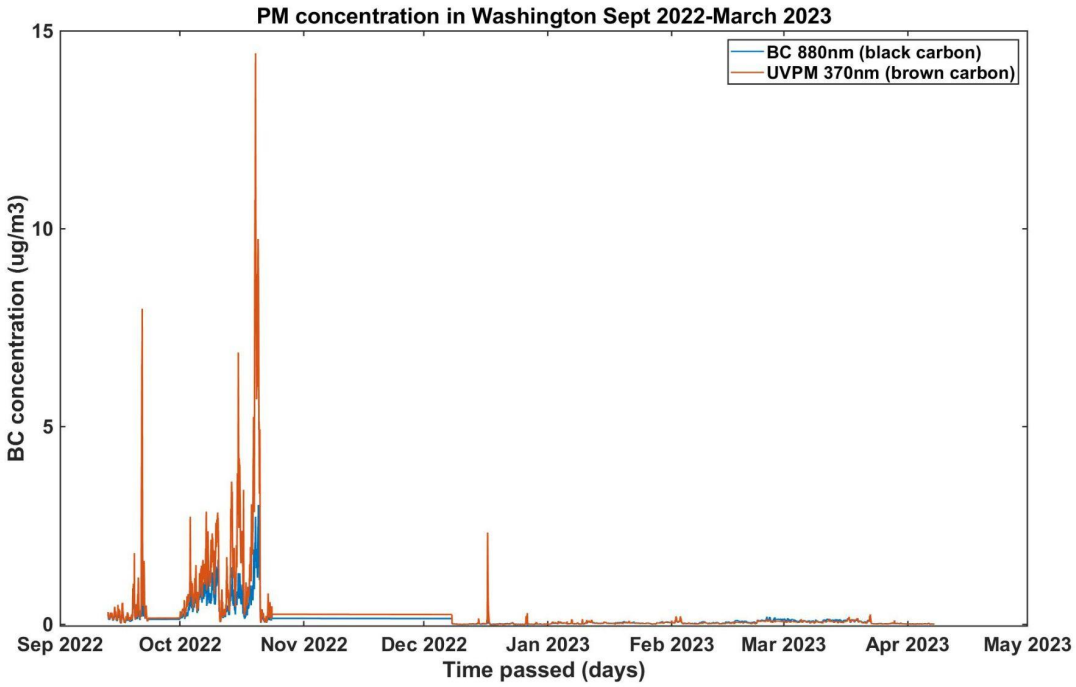

Figure 6: Aethalometer time series from September 2022-April 2023 of black carbon (blue) and brown carbon (red) in μg/m^3. September-November values were recorded at the UW Thornton lab in Seattle, and values from January-May were recorded at the CPO field site. The blank between November and December was during the installation period when the instrument was not recording.

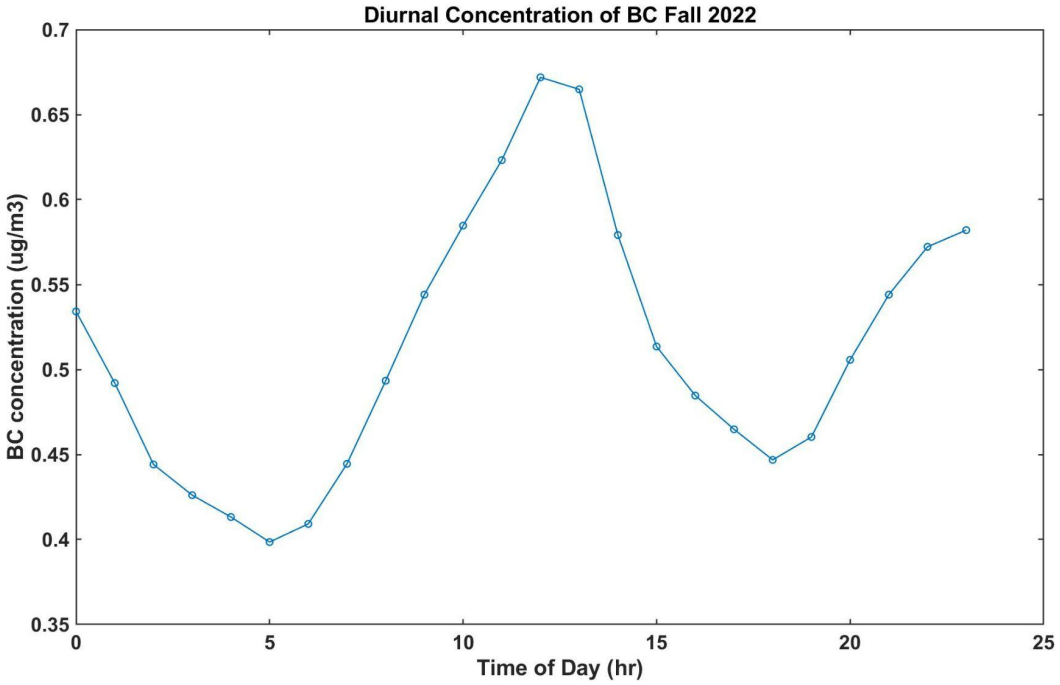

Figure 7: The diurnal cycle of black carbon from September-December 2022 in Seattle, WA, in ug/m3. There is a clear decrease during the nighttime hours and an increase during the daytime potentially from fossil fuel combustion.

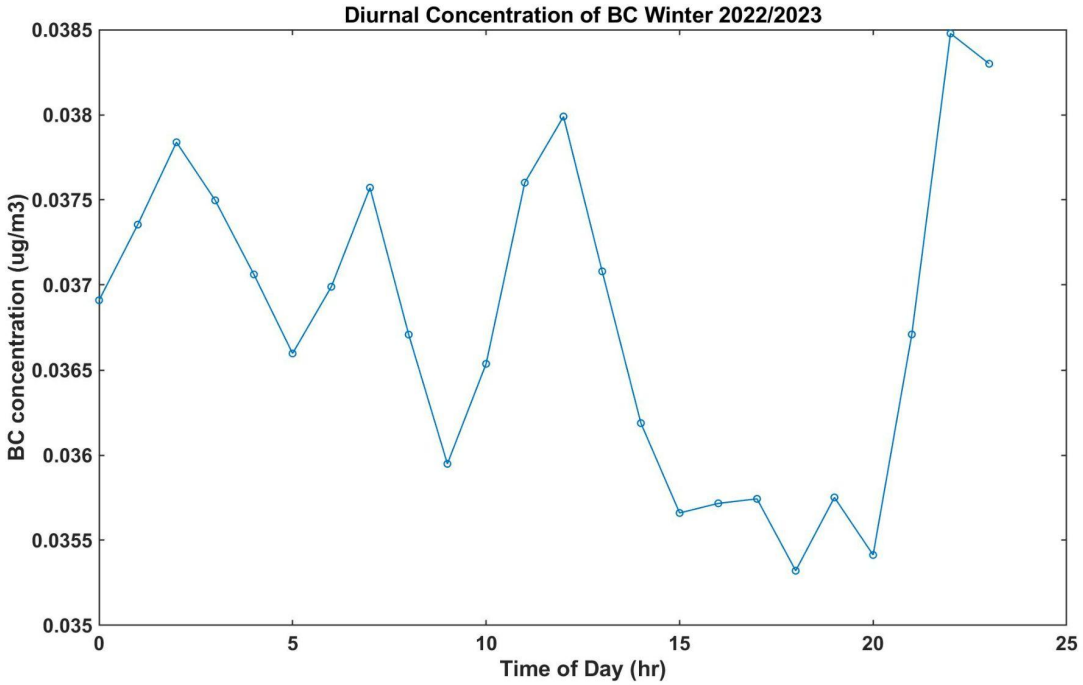

Figure 8: The diurnal cycle of black carbon from December 2022-February 2023, measured at CPO in $\mu g/m^3$. There is no discernable diurnal pattern for the wintertime months, which was potentially skewed by large BC spikes in December.

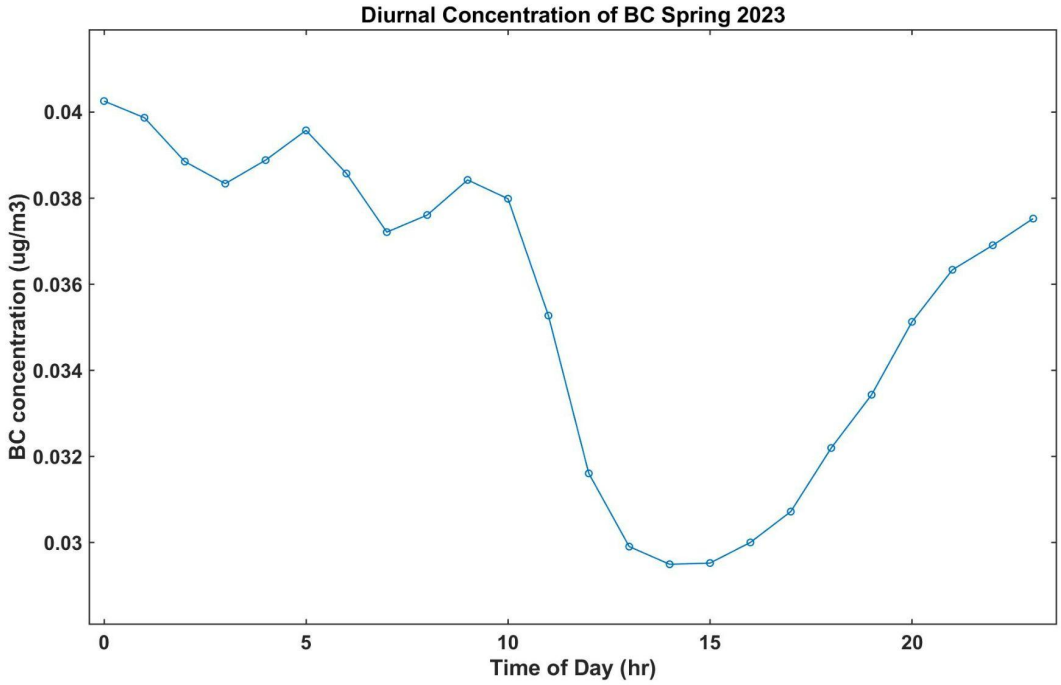

Figure 9: The diurnal cycle of black carbon from March-May 2023 at CPO in ug/m^3. Unlike the data from Seattle, the increased values are present primarily during the nighttime hours, and there is a notable decrease during the day.

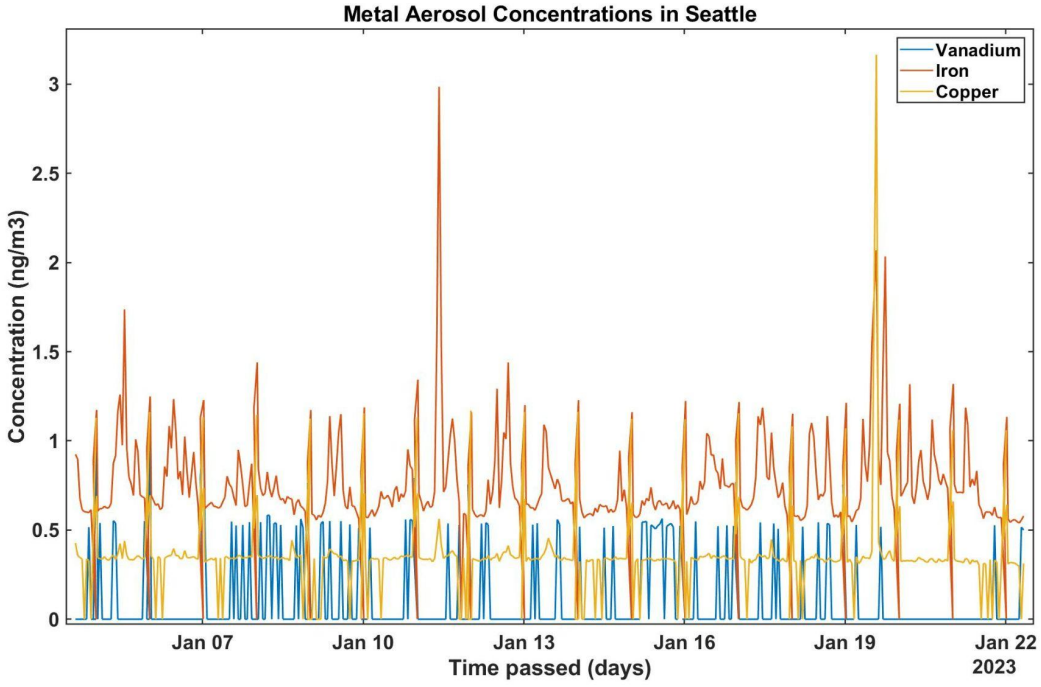

Figure 10: Xact data in January 2023 recorded in Seattle, WA. Three common metals are shown, Vanadium (blue), Iron (red), and Copper (yellow) in ng/m^3.

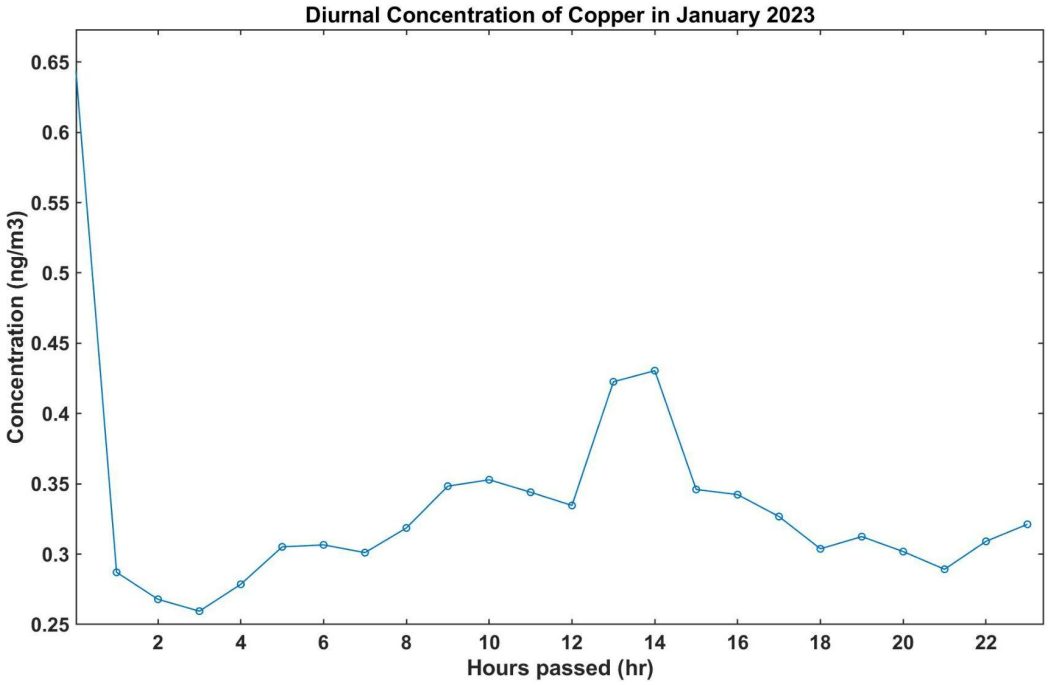

Figure 11: The diurnal cycle of Copper in January 2023 in ng/m^3. There is an elevation in concentration observed during the daytime hours when people are most likely to be in the lab.

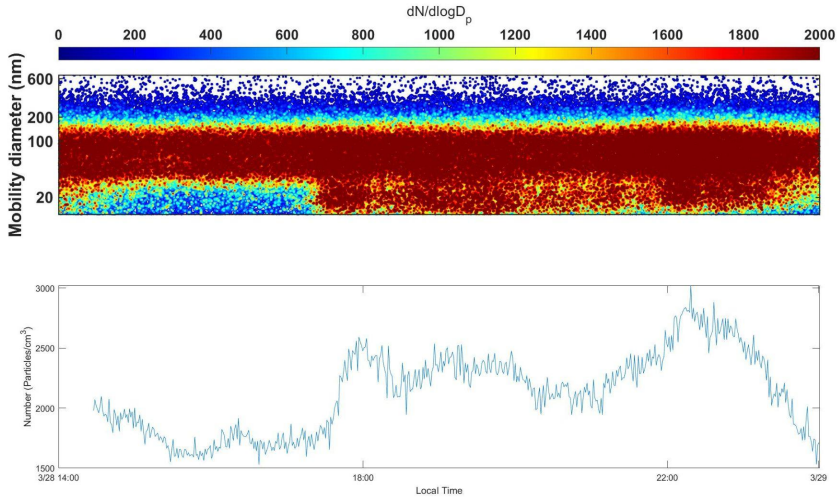

Figure 12: SMPS time series during 3/29/2023. The top plot shows the concentration over time based on different particle diameters, with higher concentrations in red and lower in blue. The diameter is recorded in nm and the concentration in dN/dlogDp. The bottom plot is the total concentration of particulate matter in # particles/m^3 over time.

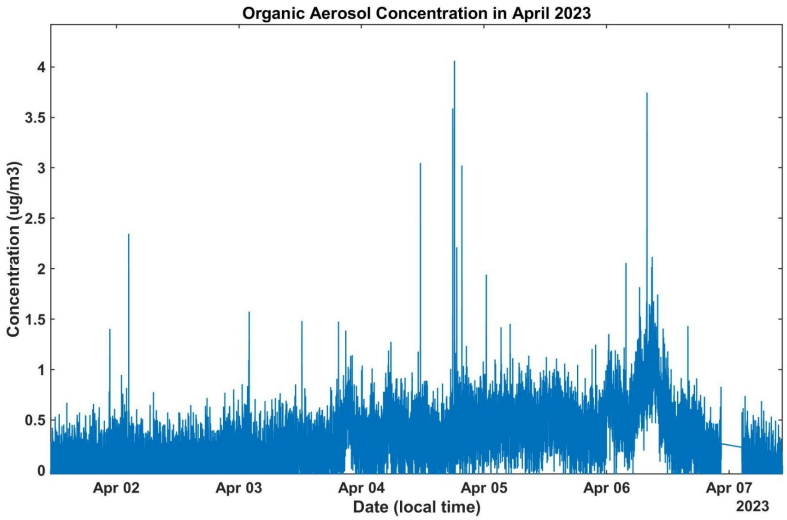

Figure 13: Time series of organic aerosol at CPO from April 1-7 2023 in μg/m^3. This time series concentration range is roughly what we expect to see from the site, given how rural the area is.

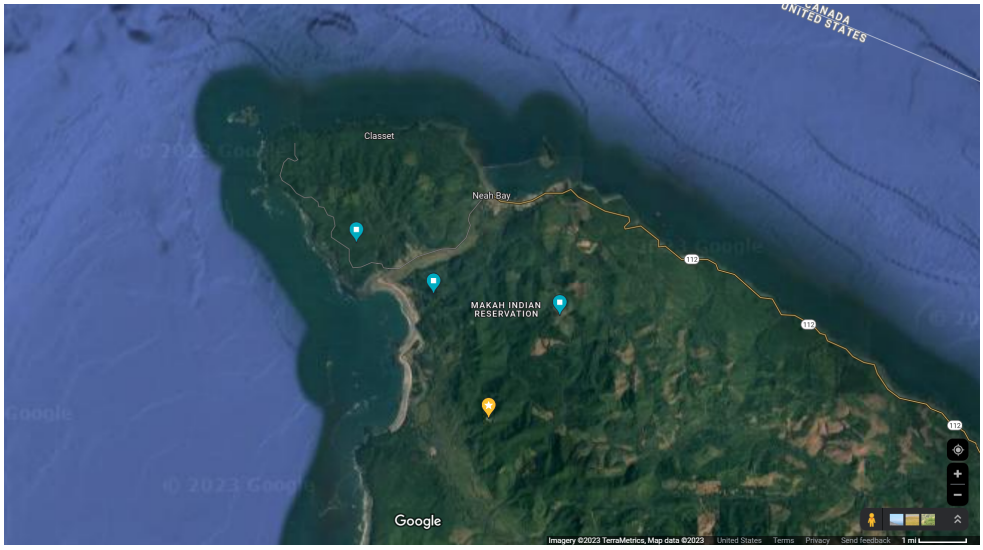

Figure 14: Location of the fires on November 17, 2022 (blue markers) compared to the field site location (yellow pin).

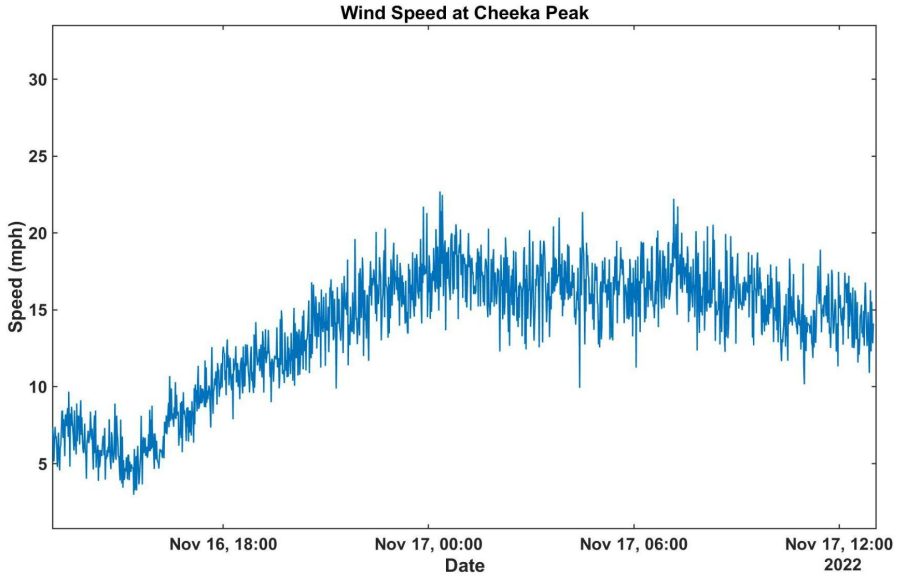

Figure 15: Wind speed at the CPO field site from November 16-17th, 2022, in miles per hour.

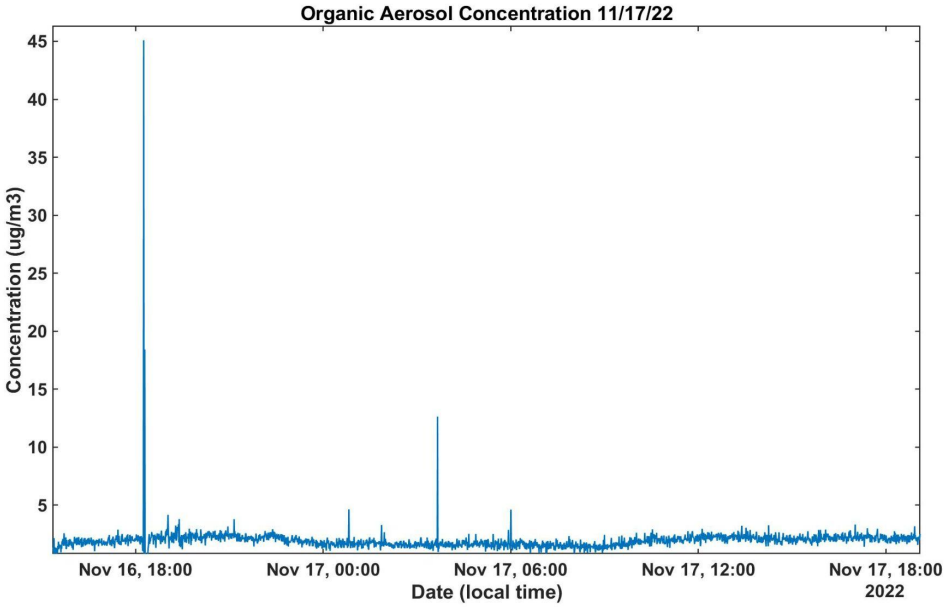

Figure 16: Time series of organic aerosols from the ACSM from November 16-17th, 2022, measured in μg/m3. The fire signal can be seen as a large spike in the late evening of the 16th and early morning of the 17th.

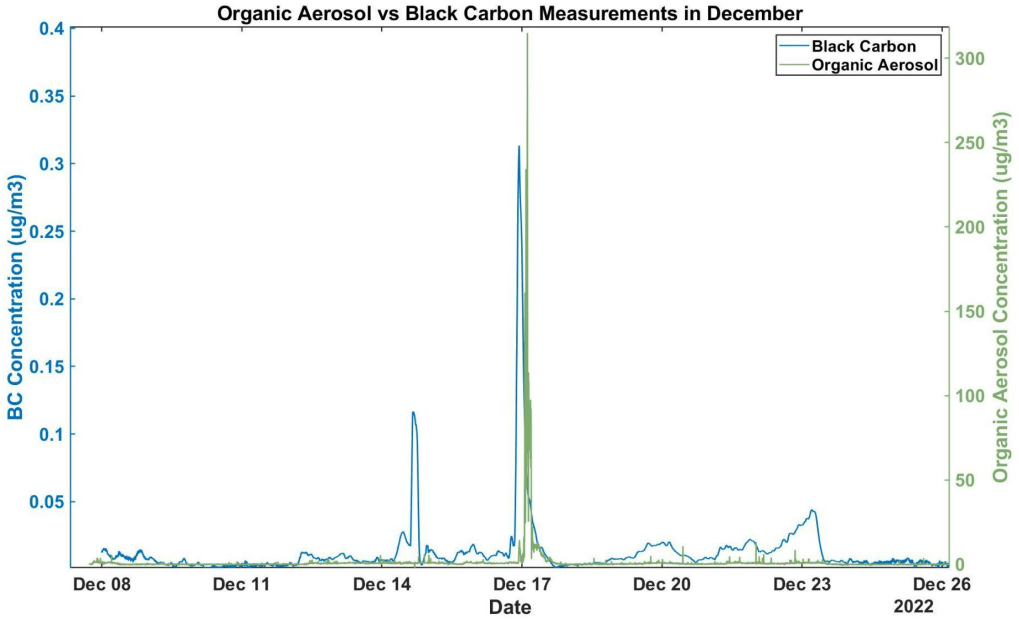

Figure 17: Time series of organic aerosols in green (ACSM) compared to black carbon in blue (aethalometer) over the month of December 2022. Both sets of data are measured in ug/m^3. It is clear that the aerosol event matches between the two instruments and occurred at the same time.

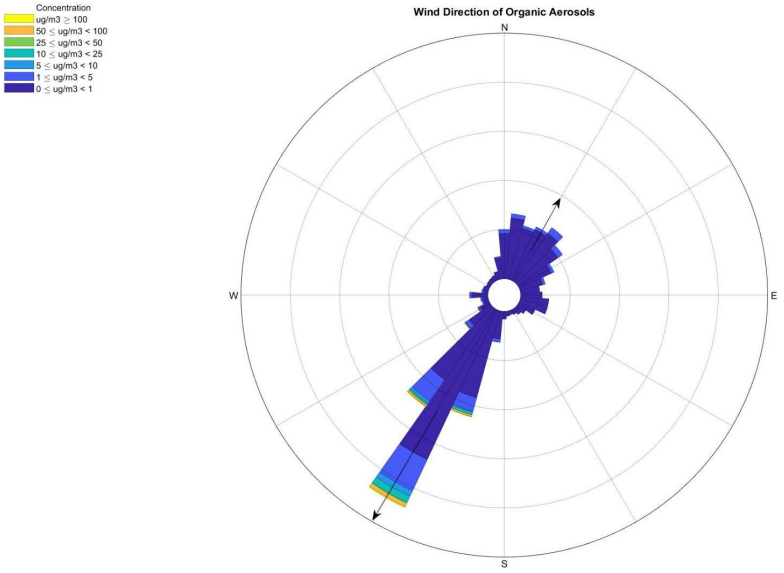

Figure 18: Wind rose of organic aerosol concentration in μg/m^3 correlated with wind direction on December 17th. Most of the wind, including the wind that brought the largest concentration of aerosols, originated from the NE, off the coast.

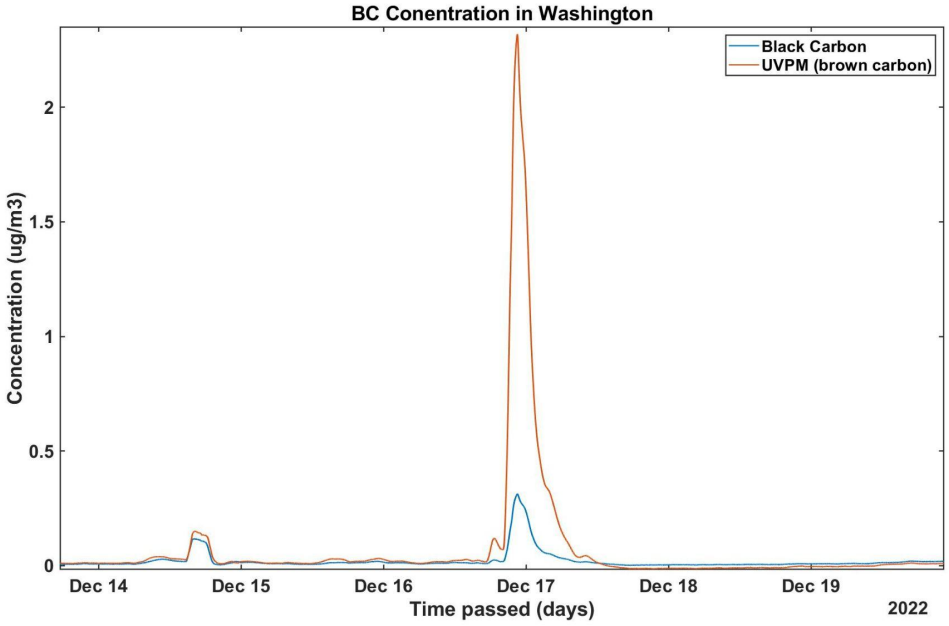

Figure 19: Time series of black (blue) and brown (red) carbon during December 2022 measured in μg/m^3. High ratios of brown to black carbon indicate biomass burning.

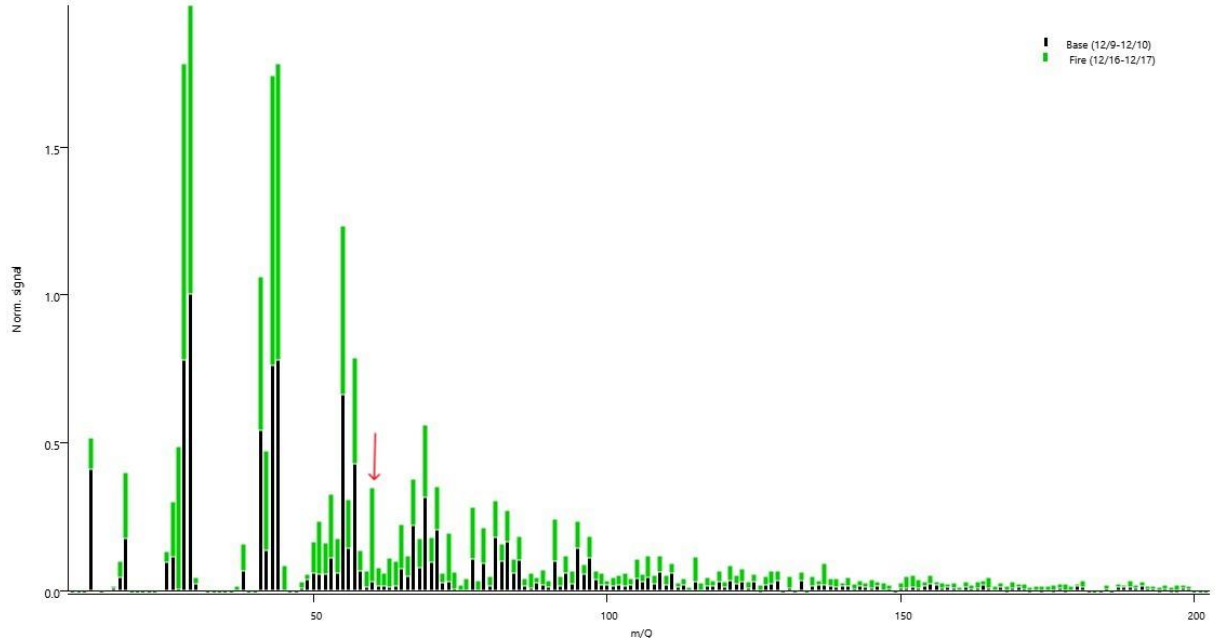

Figure 20: Mass spectrum of the December aerosol event (green) and the base levels that occurred for the majority of the rest of December (black). There is a clear elevation of signal overall. However, more notably, there is an enhancement of C60 (red arrow), which corresponds to the biomass-burning tracer levoglucosan.

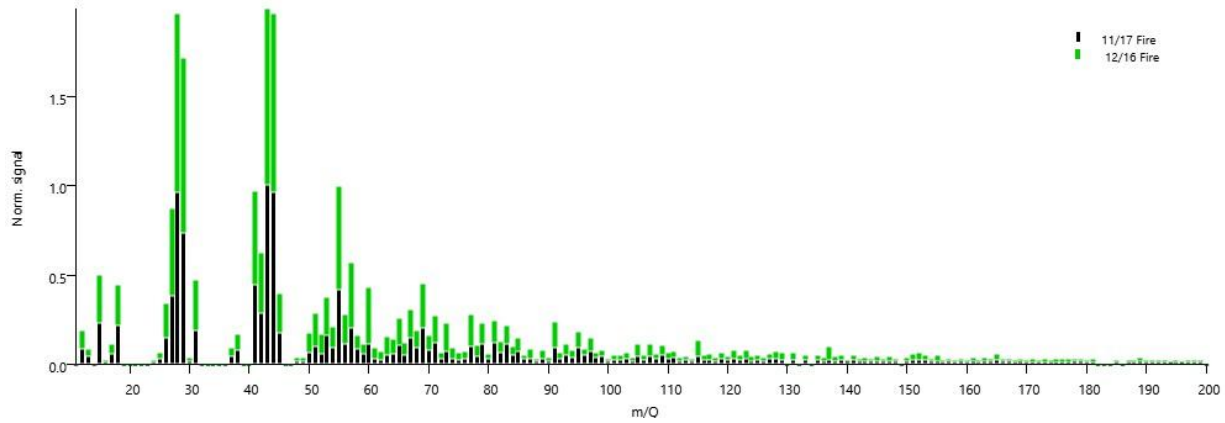

Figure 21: Mass spectrum of the December aerosol event (green) and the November fire (black). Though there are overall signal differences, the characteristics of both events match almost exactly.

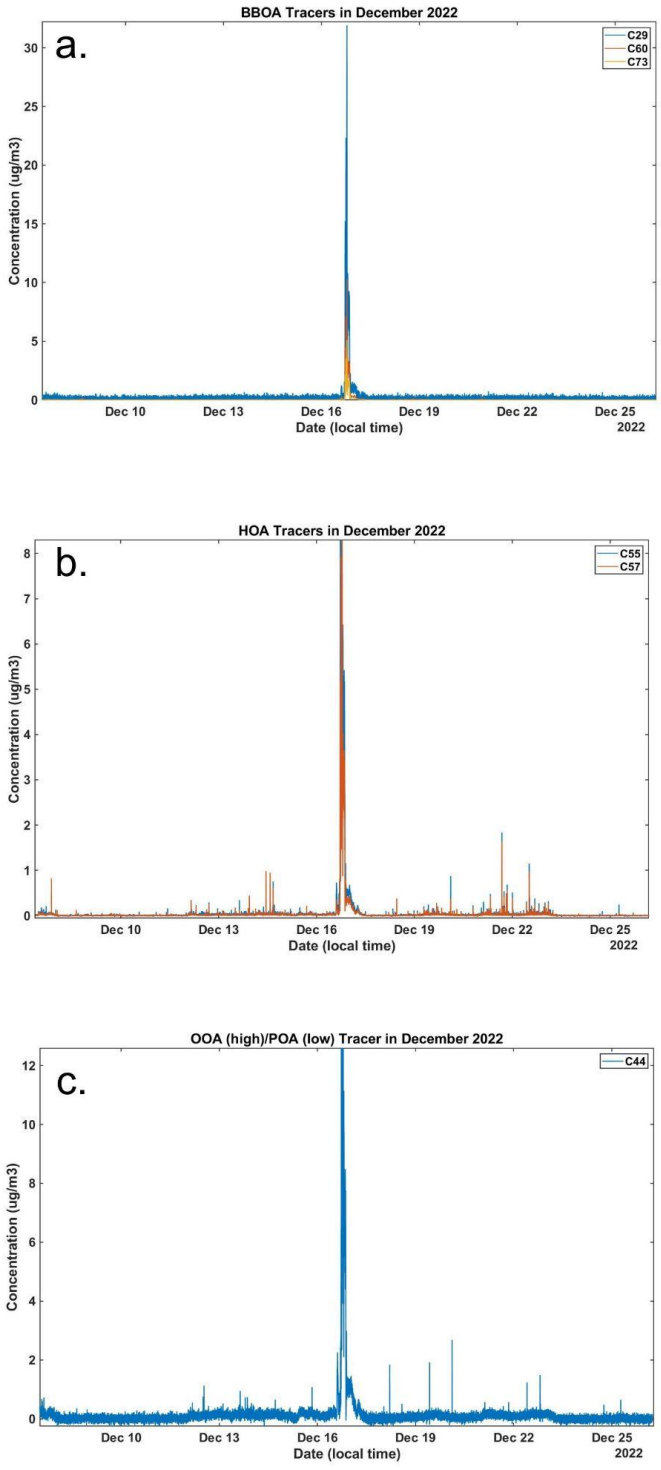

Figure 22: Time series of the basic a. BBOA, b. HOA, and c. OOA tracers from the ACSM during December 2022. All species are measured in g/m3.

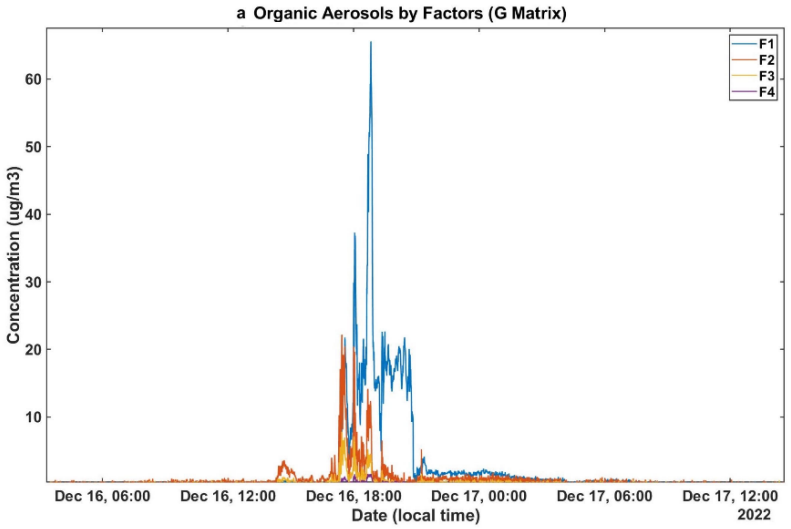
a Organic Aerosols by Factors (G Matrix)
F1
F2
F3
F4
Concentration (ug/m3)
60
50
40
30
20
10
Dec 16, 06:00
Dec 16, 12:00
Dec 16, 18:00
Dec 17, 00:00
Dec 17, 06:00
Dec 17, 12:00
Date (local time)
2022

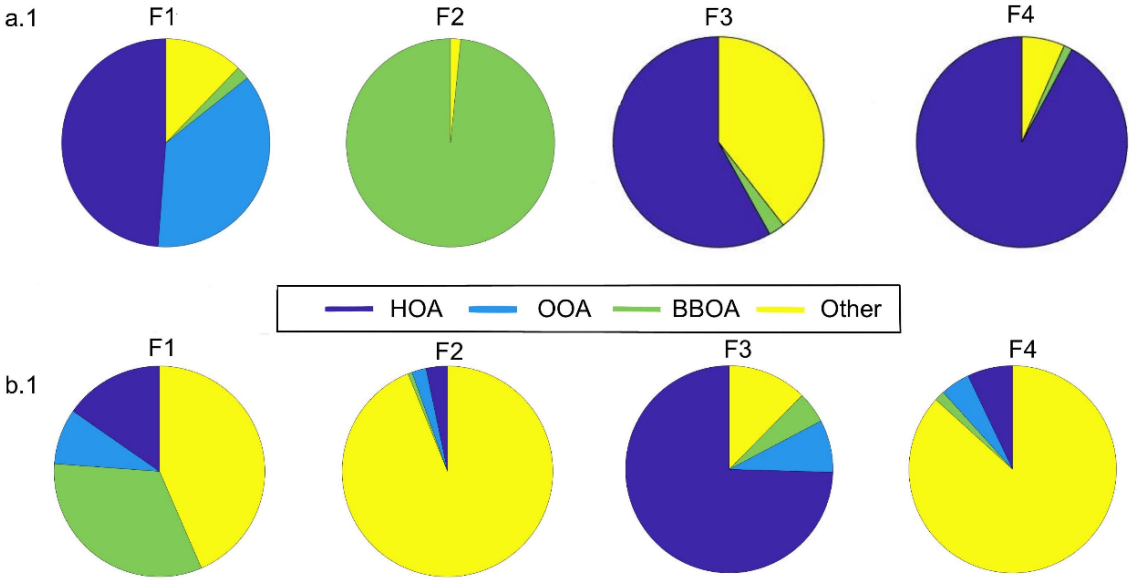
a.1
F1
F2
F3
F4
HOA
OOA
BBOA
Other
b.1
F1
F2
F3
F4

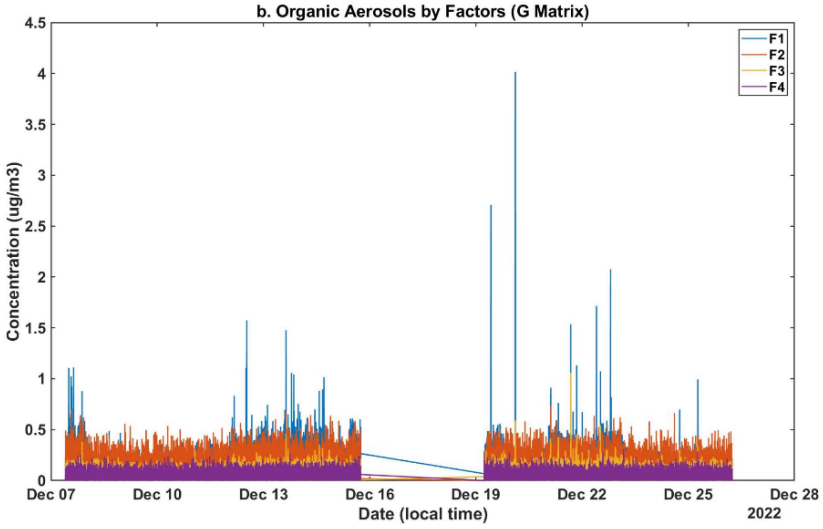
b. Organic Aerosols by Factors (G Matrix)
F1
F2
F3
F4
Concentration (ug/m3)
4.5
4
3.5
3
2.5
2
1.5
1
0.5
0
Dec 07
Dec 10
Dec 13
Dec 16
Dec 19
Dec 22
Dec 25
Dec 28
Date (local time)
2022

Figure 23: Time series of the NNMF G matrix and its four factors for the December 2022 aerosol event (a), and the background spectra (b). The pie charts show the composition breakdown of each factor by OA category: BBOA (green), HOA (purple), OOA (blue). A.1 shows the compositions of the factors from just the fire, and b.1 shows the composition of the factors from the background spectrum.

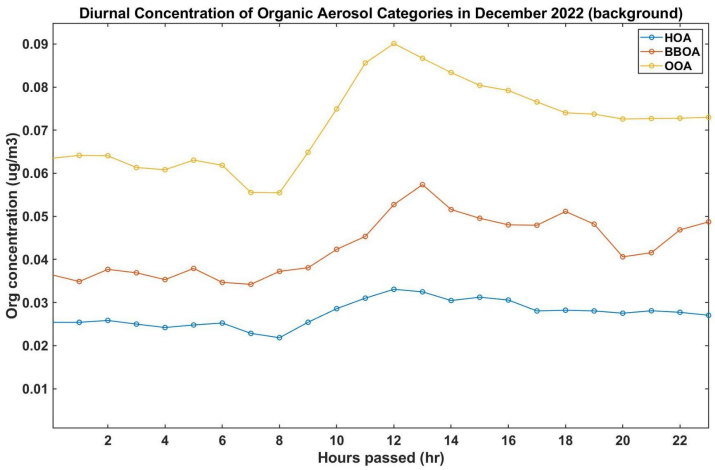

Figure 24: Diurnal cycles of each OA category from the ACSM at CPO: HOA (blue), BBOA (red), and OOA (yellow).

References

1. *About | ASCENT*. ascent.research.gatech.edu. https://ascent.research.gatech.edu/about (accessed 2023-05-04).
2. *Aerosols: Tiny Particles, Big Impact*. Nasa.gov. https://earthobservatory.nasa.gov/features/Aerosols/page3.php (accessed 2023-04-16).
3. Alghamdi, A. G.; EL-Saeid, M. H.; Alzahrani, A. J.; Ibrahim, H. M. Heavy Metal Pollution and Associated Health Risk Assessment of Urban Dust in Riyadh, Saudi Arabia. *PLOS ONE* **2022**, *17* (1), e0261957. https://doi.org/10.1371/journal.pone.0261957.

4. *Atmospheric Aerosols: What Are They, and Why Are They So Important?* NASA. https://www.nasa.gov/centers/langley/news/factsheets/Aerosols.html (accessed 2023-04-19).
5. Bernd R.T. Simoneit; Schauer, J. J.; Nolte, C. G.; Oros, D. R.; Elias, V. O.; Fraser, M.; Rogge, W. F.; Cass, G. R. Levoglucosan, a Tracer for Cellulose in Biomass Burning and Atmospheric Particles. *Atmospheric Environment* **1999**, *33* (2), 173–182. https://doi.org/10.1016/s1352-2310(98)00145-9.
6. Bertschi, I. T.; Jaffe, D. Long-Range Transport of Ozone, Carbon Monoxide, and Aerosols to the NE Pacific Troposphere during the Summer of 2003: Observations of Smoke Plumes from Asian Boreal Fires. *Journal of Geophysical Research* **2005**, *110* (D5). https://doi.org/10.1029/2004jd005135.
7. Bressi, M.; Cavalli, F.; Putaud, J.-P.; Froelich, R.; Petit, J. E.; Aas, W.; Aijala, M.; Alastuey, A.; Allan, J. D.; Aurela, M.; Berico, M.; Bougiatioti, A.; Bukowiecki, N.; Canonaco, F.; Crenn, V.; Dusanter, S.; Ehn, M.; Elsasser, M.; Flentje, H.; Graf, P. *A European aerosol phenomenology -7: High-time resolution chemical characteristics of submicron particulate matter across Europe*. JRC Publications Repository. https://publications.jrc.ec.europa.eu/repository/handle/JRC121373 (accessed 2023-05-04).
8. Bruns, E. A.; PerraudV.; Zelenyuk, A.; Ezell, M. J.; Johnson, S. N.; Yu, Y.; Imre, D.; Finlayson-Pitts, B. J.; Alexander, M. L. Comparison of FTIR and Particle Mass Spectrometry for the Measurement of Particulate Organic Nitrates. *Environmental Science & Technology* **2010**, *44* (3), 1056–1061. https://doi.org/10.1021/es9029864.

9. Cao, G.; Yan, Y.; Zou, X.; Zhu, R.; Ouyang, F. Applications of Infrared Spectroscopy in Analysis of Organic Aerosols. *Spectral Analysis Review* **2017**, *6* (1), 12–32. https://doi.org/10.4236/sar.2018.61002.
10. Corbin, J. C.; Mensah, A. A.; Pieber, S. M.; Orasche, J.; Michalke, B.; Zanatta, M.; Czech, H.; Massabò, D.; Buatier de Mongeot, F.; Mennucci, C.; El Haddad, I.; Kumar, N. K.; Stengel, B.; Huang, Y.; Zimmermann, R.; Prévôt, A. S. H.; Gysel, M. Trace Metals in Soot and $PM_{2.5}$ from Heavy-Fuel-Oil Combustion in a Marine Engine. *Environmental Science & Technology* **2018**, *52* (11), 6714–6722. https://doi.org/10.1021/acs.est.8b01764.
11. Cubison, M. J.; Ortega, A.; Hayes, P. M.; Farmer, D. K.; Day, D. A.; Lechner, M. J.; Brune, W. H.; Apel, E. C.; Diskin, G. S.; Fisher, J. A.; Fuelberg, H. E.; Arsineh Hecobian; Knapp, D. J.; Mikoviny, T.; Riemer, D. D.; Sachse, G. W.; Sessions, W. R.; Weber, R. J.; Weinheimer, A. J.; Armin Wisthaler. Effects of Aging on Organic Aerosol from Open Biomass Burning Smoke in Aircraft and Laboratory Studies. *Atmospheric Chemistry and Physics* **2011**, *11* (23), 12049–12064. https://doi.org/10.5194/acp-11-12049-2011.
12. Dao, X.; Lin, Y.-C.; Cao, F.; Di, S.-Y.; Hong, Y.; Xing, G.; Li, J.; Fu, P.; Zhang, Y.-L. Introduction to the National Aerosol Chemical Composition Monitoring Network of China: Objectives, Current Status, and Outlook. *Bulletin of the American Meteorological Society* **2019**, *100* (12), ES337–ES351. https://doi.org/10.1175/BAMS-D-18-0325.1.
13. Fröhlich, R.; Cubison, M. J.; Slowik, J. G.; Bukowiecki, N.; André S. H. Prévôt; Urs Baltensperger; Schneider, J. M.; Kimmel, J. R.; M. Gonin; Rohner, U.; Worsnop, D. R.; Jayne, J. T. The ToF-ACSM: A Portable Aerosol Chemical Speciation Monitor with

TOFMS Detection. *Atmospheric Measurement Techniques* **2013**, *6* (11), 3225–3241. https://doi.org/10.5194/amt-6-3225-2013.

14. George, K. M.; Ruthenburg, T. C.; Smith, J.; Yu, L.; Zhang, Q.; Anastasio, C.; Dillner, A. M. FT-IR Quantification of the Carbonyl Functional Group in Aqueous-Phase Secondary Organic Aerosol from Phenols. *Atmospheric Environment* **2015**, *100*, 230–237. https://doi.org/10.1016/j.atmosenv.2014.11.011.
15. Genualdi, S.; Killin, R. K.; Woods, J.; Wilson, G. D.; Schmedding, D.; Massey, S. L. Trans-Pacific and Regional Atmospheric Transport of Polycyclic Aromatic Hydrocarbons and Pesticides in Biomass Burning Emissions to Western North America. *Environmental Science & Technology* **2009**, *43* (4), 1061–1066. https://doi.org/10.1021/es802163c.
16. Goetz, J. D.; Giordano, M. R.; Stockwell, C. E.; Bhave, P. V.; Puppala, P. S.; Panday, A. K.; Jayarathne, T.; Stone, E. A.; Yokelson, R. J.; DeCarlo, P. F. Aerosol Mass Spectral Profiles from NAMaSTE Field-Sampled South Asian Combustion Sources. *ACS Earth and Space Chemistry* **2022**, *6* (11), 2619–2631. https://doi.org/10.1021/acsearthspacechem.2c00173.
17. Gupta, T.; Rajeev, P.; Rajput, R. Emerging Major Role of Organic Aerosols in Explaining the Occurrence, Frequency, and Magnitude of Haze and Fog Episodes during Wintertime in the Indo Gangetic Plain. *ACS Omega* **2022**, *7* (2), 1575–1584. https://doi.org/10.1021/acsomega.1c05467.
18. Hadley, O. L. Background PM2.5 Source Apportionment in the Remote Northwestern United States. *Atmospheric Environment* **2017**, *167*, 298–308. https://doi.org/10.1016/j.atmosenv.2017.08.030.

19. Hansen, A.; Schnell, R. C. *Magee Scientific the Aethalometer ™*; 2005. https://www.psi.ch/sites/default/files/import/lac/ProjectAddonCatcosOperationsEN/Aethalometer_book_2005.07.02.pdf (accessed 2023-05-04).
20. He, Q.; Ding, X.; Fu, X.; Zhang, Y.; Wang, J.; Liu, Y.; Tang, M.; Wang, X.; Rudich, Y. Secondary Organic Aerosol Formation from Isoprene Epoxides in the Pearl River Delta, South China: IEPOX‐ and HMML‐Derived Tracers. *Journal of Geophysical Research: Atmospheres* **2018**, *123* (13), 6999–7012. https://doi.org/10.1029/2017jd028242.
21. Husar, R. B.; Tratt, D. M.; Schichtel, B. A.; Falke, S. R.; Li, F.; Jaffe, D.; Gassó, S.; Gill, T.; Laulainen, N. S.; Lu, F.; Reheis, M. C.; Chun, Y.; Westphal, D.; Holben, B. N.; Gueymard, C.; McKendry, I.; Kuring, N.; Feldman, G. C.; McClain, C.; Frouin, R. J. Asian Dust Events of April 1998. *Journal of Geophysical Research: Atmospheres* **2001**, *106* (D16), 18317–18330. https://doi.org/10.1029/2000jd900788.
22. *IMPROVE Program*. vista.cira.colostate.edu. https://vista.cira.colostate.edu/Improve/improve-program/ (accessed 2023-04-28).
23. KING 5 Staff. *Evacuations lifted after 3 fires break out near Neah Bay*. king5.com. https://www.king5.com/article/news/local/evacuations-fires-neah-bay/281-a616dac2-d41b-4566-b408-49c7538e0663 (accessed 2023-05-02).
24. Kuang, C. *TSI Model 3936 Scanning Mobility Particle Spectrometer Instrument Handbook*. www.osti.gov. https://www.osti.gov/biblio/1245993 (accessed 2023-05-04).
25. Kulmala, M. Build a Global Earth Observatory. *Nature* **2018**, *553* (7686), 21–23. https://doi.org/10.1038/d41586-017-08967-y.
26. Lee, S.-H.; Gordon, H.; Yu, H.; Haley, R.; Li, Y.; Zhang, R.; Lehtipalo, K. New Particle Formation in the Atmosphere: From Molecular Clusters to Global Climate. *Journal Of*

Geophysical Research: Atmospheres **2019**, *124* (13), 7098–7146. https://doi.org/10.1029/2018jd029356.

27. Li, W.; Ge, P.; Chen, M.; Tang, J.; Cao, M.; Cui, Y.; Hu, K.; Nie, D. Tracers from Biomass Burning Emissions and Identification of Biomass Burning. *Atmosphere* **2021**, *12* (11), 1401. https://doi.org/10.3390/atmos12111401.
28. Lin, Y.-H. .; Knipping, E. M.; Edgerton, E. S.; Shaw, S. L.; Surratt, J. D. Investigating the Influences of so_2 and NH_3 Levels on Isoprene-Derived Secondary Organic Aerosol Formation Using Conditional Sampling Approaches. *Atmospheric Chemistry and Physics* **2013**, *13* (16), 8457–8470. https://doi.org/10.5194/acp-13-8457-2013.
29. Luo, H.; Wang, Q.; Guan, Q.; Ma, Y.; Ni, F.; Yang, E.; Zhang, J. Heavy Metal Pollution Levels, Source Apportionment and Risk Assessment in Dust Storms in Key Cities in Northwest China. *Journal of Hazardous Materials* **2021**, *422*, 126878. https://doi.org/10.1016/j.jhazmat.2021.126878.
30. M. Rami Alfarra; André S. H. Prévôt; Sönke Szidat; J. Sandradewi; Weimer, S.; Lanz, V. A.; Schreiber, D. K.; Mohr, M.; Urs Baltensperger. Identification of the Mass Spectral Signature of Organic Aerosols from Wood Burning Emissions. *Environmental Science & Technology* **2007**, *41* (16), 5770–5777. https://doi.org/10.1021/es062289b.
31. Ma, X.; von Salzen, K.; Li, J. Modelling Sea Salt Aerosol and Its Direct and Indirect Effects on Climate. *Atmospheric Chemistry and Physics* **2008**, *8* (5), 1311–1327. https://doi.org/10.5194/acp-8-1311-2008.
32. Martinsson, J.; Abdul Azeem, H.; Sporre, M. K.; Bergström, R.; Ahlberg, E.; Öström, E.; Kristensson, A.; Swietlicki, E.; Eriksson Stenström, K. Carbonaceous Aerosol Source Apportionment Using the Aethalometer Model – Evaluation by Radiocarbon and

Levoglucosan Analysis at a Rural Background Site in Southern Sweden. *Atmospheric Chemistry and Physics* **2017**, *17* (6), 4265–4281. https://doi.org/10.5194/acp-17-4265-2017.

33. Myhre, G.; Myhre, C.; Samset, E. L.; Storelvmo, T. *Aerosols and their Relation to Global Climate and Climate Sensitivity | Learn Science at Scitable*. www.nature.com. https://www.nature.com/scitable/knowledge/library/aerosols-and-their-relation-to-global-climate-102215345/#:~:text=Aerosols%20are%20vital%20for%20cloud (accessed 2023-04-15).
34. National Academies of Sciences, E. *The Future of Atmospheric Chemistry Research: Remembering Yesterday, Understanding Today, Anticipating Tomorrow*; The National Academies Press , 2016.
35. *NCore Monitoring Network*. www.epa.gov. https://www.epa.gov/amtic/ncore-monitoring-network (accessed 2023-04-28).
36. Ng, N. L.; Canagaratna, M. R.; Jimenez, J. L.; Zhang, Q.; Ulbrich, I. M.; Worsnop, D. R. Real-Time Methods for Estimating Organic Component Mass Concentrations from Aerosol Mass Spectrometer Data. *Environmental Science & Technology* **2011**, *45* (3), 910–916. https://doi.org/10.1021/es102951k.
37. Ng, N. L.; Herndon, S. C.; Trimborn, A.; Canagaratna, M. R.; Croteau, P.; Onasch, T. B.; Sueper, D.; Worsnop, D. R.; Zhang, Q.; Sun, Y.; Jayne, J. T. An Aerosol Chemical Speciation Monitor (ACSM) for Routine Monitoring of the Composition and Mass Concentrations of Ambient Aerosol. *Aerosol Science and Technology* **2011**, *45* (7), 780–794. https://doi.org/10.1080/02786826.2011.560211.

38. Olson, M. F.; Mercedes Victoria Garcia; Robinson, M. E.; Paul Van Rooy; Dietenberger, M. A.; Bergin, M. H.; Schauer, J. J. Investigation of Black and Brown Carbon Multiple-Wavelength-Dependent Light Absorption from Biomass and Fossil Fuel Combustion Source Emissions. 2015, 120 (13), 6682–6697. https://doi.org/10.1002/2014jd022970.

39. Osaka, S. Why Seattle Currently Has the Worst Air Quality in the World. *Washington Post*. October 20, 2022. https://www.washingtonpost.com/climate-environment/2022/10/20/seattle-air-quality-worst-in-world/.

40. Peltola, M.; Rose, C.; Trueblood, J. V.; Gray, S.; Harvey, M.; Sellegri, K. New Particle Formation in Coastal New Zealand with a Focus on Open-Ocean Air Masses. *Atmospheric Chemistry and Physics* **2022**, *22* (9), 6231–6254. https://doi.org/10.5194/acp-22-6231-2022.

41. Su, P.; Joutsensaari, J.; Dada, L.; Zaidan, M. A.; Nieminen, T.; Li, X.; Wu, Y.; Decesari, S.; Tarkoma, S.; Petäjä, T.; Kulmala, M.; Pellikka, P. New Particle Formation Event Detection with Mask R-CNN. *Atmospheric Chemistry and Physics* **2022**, *22* (2), 1293–1309. https://doi.org/10.5194/acp-22-1293-2022.

42. Suzuki, Y.; Matsunaga, K.; Yamashita, Y. Assignment of PM2.5 Sources in Western Japan by Non-Negative Matrix Factorization of Concentration-Weighted Trajectories of GED-ICP-MS/MS Element Concentrations. *Environmental Pollution* **2021**, *270*, 116054. https://doi.org/10.1016/j.envpol.2020.116054.

43. United States Environmental Protection Agency. *Health and Environmental Effects of Particulate Matter (PM)*. US EPA.

https://www.epa.gov/pm-pollution/health-and-environmental-effects-particulate-matter-pm (accessed 2023-04-18).

44. US EPA, O. Chemical Speciation Network - Parameters Reported to the Air Quality System (AQS). www.epa.gov. https://www.epa.gov/amtic/chemical-speciation-network-parameters-reported-air-quality-system-aqs (accessed 2023-06-01).
45. Virtanen , A. *Secondary Organic Aerosol (SOA) Formation, Properties and Evolution in the Atmosphere*. www.mdpi.com. https://www.mdpi.com/journal/atmosphere/special_issues/SOA_Atmosphere (accessed 2021-10-24).
46. *Xact® 625i Ambient Continuous Multi-Metals Monitor*. Sailbri Cooper, Inc. http://sci-monitoring.com/product/xact-625i-ambient-continuous-multi-metals-monitor/ (accessed 2023-05-04).
47. Xu, W.; He, Y.; Qiu, Y.; Chen, C.; Xie, C.; Lei, L.; Li, Z.; Sun, J.; Li, J.; Fu, P.; Wang, Z.; Worsnop, D. R.; Sun, Y. Mass Spectral Characterization of Primary Emissions and Implications in Source Apportionment of Organic Aerosol. *Atmospheric Measurement Techniques* **2020**, *13* (6), 3205–3219. https://doi.org/10.5194/amt-13-3205-2020.
48. Yue, S.; Zhu, J.; Chen, S.; Xie, Q.; Li, W.; Li, L.; Ren, H.; Su, S.; Li, P.; Ma, H.; Fan, Y.; Cheng, B.; Wu, L.; Deng, J.; Hu, W.; Ren, L.; Wei, L.; Zhao, W.; Tian, Y.; Pan, X. Brown Carbon from Biomass Burning Imposes Strong Circum-Arctic Warming. *One Earth* **2022**, *5* (3), 293–304. https://doi.org/10.1016/j.oneear.2022.02.006.
49. Zhao, J.; Zhang, Y.; Xu, H.; Tao, S.; Wang, X.; Yu, Q.; Chen, Y.; Zou, Z.; Ma, W. Trace Elements from Ocean‐Going Vessels in East Asia: Vanadium and Nickel Emissions and

Their Impacts on Air Quality. *Journal Of Geophysical Research: Atmospheres* **2021**, *126* (8). https://doi.org/10.1029/2020jd033984.